Intermetallics 107 (2019) 39–46

Contents lists available at ScienceDirect

Intermetallics

journal homepage: www.elsevier.com/locate/intermet

Enhanced irradiation resistance of amorphous alloys by introducing amorphous/amorphous interfaces

L. Huang[a,1], Z.Q. Chen[b,1], W.B. Liu[c], P. Huang[a,*], X.K. Meng[b], K.W. Xu[a], F. Wang[d,**], T.J. Lu[e,d]

[a] State Key Laboratory for Mechanical Behavior of Material, Xi'an Jiaotong University, PR China
[b] Institute of Materials Engineering, National Laboratory of Solid State Microstructures, Collaborative Innovation Center of Advanced Microstructures, Nanjing University, PR China
[c] Department of Nuclear Science and Technology, Xi'an Jiaotong University, PR China
[d] State Key Laboratory for Strength and Vibration of Mechanical Structures, Xi'an Jiaotong University, PR China
[e] State Key Laboratory of Mechanics and Control of Mechanical Structures, Nanjing University of Aeronautics and Astronautics, PR China

ARTICLE INFO

Keywords:
Irradiation resistance
Amorphous alloys
Nanolaminates
Interface
Microstructure

ABSTRACT

To clarify the effect of amorphous/amorphous (A/A) interfaces during ion irradiation, the He ion irradiation responses of ZrCu/ZrCuNiAlSi A/A nanolaminates (A/ANLs) as well as ZrCu and ZrCuNiAlSi single-layered amorphous thin films were examined. The results showed the A/ANLs exhibited superior irradiation resistance compared with the corresponding single-layered thin films, as the former possessed better microstructure stability and higher He ion solubility than the latter during He ion irradiation. Besides, A/ANLs having more interfaces exhibited even better irradiation resistance than those having less. The enhanced irradiation resistance of A/ANLs was attributed to the sink effect of A/A interfaces, which effectively reduced the amount of radiation-induced "defects" and He bubbles.

1. Introduction

The development of irradiation tolerant materials is of crucial importance for the next-generation nuclear energy technology, as these materials can endure the harsh environments in the fusion reactor without significant structural changes and serious mechanical degradation [1–3]. One of the effective approaches is to introduce affluent interfaces by preparing materials in the form of nanolaminates, as the interfaces may serve as defect sinks to alleviate radiation damage and inhibit radiation-induced structural and property changes.

Previously, ion irradiation studies on nanolaminates focused mainly on crystalline/crystalline (C/C) interfaces, such as incoherent Cu/Nb [4], Cu/V [5], Cu/Mo [6], Cu/W [7], Al/Nb [8] and Ag/V [9], and coherent Cu/Ni [10], Cu/Co [11], Ag/Ni [12] and Fe/W [13]. It has been revealed that incoherent interfaces have higher sink strength than the coherent ones for removing radiation damages, for they can more easily recover from radiation-induced intermixing [14,15]. Moreover, the sink strength is positively related to the amount of free volume produced by incoherent interfaces, according to Molecular Dynamics (MD) simulations [16]. Thence, amorphous/crystalline (A/C) interfaces, such as CuZr/Cu [17], SiOC/Fe [18], Fe_2Zr/Fe [19], a-Y_2O_3/Fe [20] and TiO_2/Fe [21], have also been evaluated and proven as efficient sinks for mitigating radiation damages, as amorphous materials have a higher amount of free volume than their crystalline counterparts. Then, we may ask: are amorphous/amorphous (A/A) interfaces efficient for alleviating radiation damages? To our best knowledge, there exist few studies evaluating the effect of A/A interfaces during ion irradiation.

Amorphous alloys possess numerous attractive properties, such as high strength, high elastic strain limits and good wear/corrosion resistance [22,23]. In particular, amorphous alloys are suggested to be more suitable than traditional crystalline materials to serve in irradiation environments due to their long-range disorder structure, which can absorb more radiation-induced damage and avoid the formation of conventional crystal defects such as vacancy-interstitial pairs and dislocation loops [24–28]. Meanwhile, the long-range disorder structure makes amorphous alloys inherently brittle, the main obstacle for their practical application. It has been demonstrated that the plasticity of amorphous alloys could be enhanced by introducing interfaces [29–31]. Therefore, A/A metallic nanolaminates emerge as a promising

* Corresponding author.
** Corresponding author.
E-mail addresses: huangping@mail.xjtu.edu.cn (P. Huang), wangfei@mail.xjtu.edu.cn (F. Wang).
[1] These authors contributed equally to this work.

https://doi.org/10.1016/j.intermet.2019.01.007
Received 25 October 2018; Received in revised form 27 December 2018; Accepted 5 January 2019
Available online 12 January 2019
0966-9795/

irradiation resistant material and their irradiation resistance should be evaluated in detail.

In this study, to examine the roles of interfaces in A/A metallic nanolaminates during ion irradiation, two kinds of Zr-based amorphous alloys, *i.e.*, ZrCu and ZrCuNiAlSi, were chosen as constituents for nanolaminates construction. The He ion irradiation responses of A/A nanolaminates (A/ANLs) were compared to those of the constituent single-layered amorphous thin films. There are two reasons for selecting these materials: (i) the Zr-based amorphous alloys have been well studied and are easy to fabricate, with good engineering properties [32]; (ii) binary and multivariate Zr-based amorphous alloys have apparently different glass-forming abilities and thermal stabilities [33], thus different irradiation resistances [34], which is beneficial for displaying the effect of A/A interfaces.

2. Experiment methods

ZrCu and ZrCuNiAlSi single-layered amorphous thin films, as well as ZrCu/ZrCuNiAlSi A/ANLs, were deposited on Si (100) substrates by magnetron sputtering at room temperature. The A/ANLs with equal modulation have individual layer thickness of either ~25 nm or 5 nm, referred to below as A/ANLs 25 and A/ANLs 5 hereafter, respectively. The first layer on Si substrate was ZrCu and the top layer was ZrCuNiAlSi for both A/ANLs. For all the samples, the total film thickness was fixed at ~900 nm. Nominal compositions of the ZrCu and ZrCuNiAlSi amorphous thin films were $Zr_{50}Cu_{50}$ and $Zr_{61}Cu_{17.5}Ni_{10}Al_{7.5}Si_4$ (at.%) respectively, as verified by energy dispersive X-ray (EDX) analysis. The vacuum background pressure was less than 6.3×10^{-5} Pa, while the working Ar pressure was maintained at $\sim 5.4 \times 10^{-1}$ Pa. For all the samples, the deposition rate was ~ 5 nm/min. Implantation experiments were performed at room temperature using a He ion energy of 160 keV with total fluences of 2×10^{16} and 1×10^{17} ions/cm^2 at a constant beam current of ~2.5 μA. The radiation pressure was maintained at $\sim 1 \times 10^{-4}$ Pa. Prior to He irradiation, the irradiation damage profile was calculated using the Stopping and Range of Ions in Matter 2013 (SRIM-2013) software in "quick K-P mode" with a threshold energy for Zr of 40 eV, Cu of 25 eV, Ni of 40 eV, Al of 16 eV and Si of 15 eV, and the He concentration profile was calculated in "full Damage F-C mode" [35]. The maximum implantation depth was ~900 nm and the maximum He concentration was reached at the depth of 500–600 nm for all the samples, as shown in Figs. 3(a), 4(a) and 5(a) and 6(a). Note that, for simulation, the A/ANLs were simplified as alloying of $Zr_{50}Cu_{50}$ and $Zr_{61}Cu_{17.5}Ni_{10}Al_{7.5}Si_4$.

The phase structure of both unirradiated and irradiated samples was characterized by X-ray diffraction (XRD) with Cu Ka radiation (XRD-7000 Shimadzu Corporation), while their internal microstructure features were examined with high resolution transmission electron microscopy (HRTEM, JEOL JEM-2100F) operating at 200 KV. Cross-sectional TEM specimens were prepared using standard mechanical grinding, followed by low-energy ion milling. Surface morphology was characterized with scanning electron microscope (SEM, SU6600).

3. Results and discussion

3.1. Microstructure evolution of ZrCu, ZrCuNiAlSi and their A/ANLs under He irradiation

Fig. 1 displayed the XRD patterns of ZrCu, ZrCuNiAlSi, A/ANLs 25 and A/ANLs 5 samples before and after He ion irradiation. All the original samples possessed amorphous nature, since only one broad diffraction peak could be observed in each pattern. In contrast, for ZrCu amorphous thin films, the diffraction peak broadened so sharply that it almost disappeared after irradiation and a weak crystalline peak corresponding to $Cu_{10}Zr_7$ phase appeared when the fluence was increased to 1×10^{17} ions/cm^2 [Fig. 1(a)]. This indicated that radiation-induced crystallization occurred. For ZrCuNiAlSi amorphous thin films [Fig. 1(b)], no such crystallization occurred as no crystalline peak appeared in their patterns, meaning ZrCuNiAlSi might be more irradiation resistant than ZrCu. Meanwhile, the diffraction peak broadened obviously when irradiated at a fluence of 2×10^{16} ions/cm^2 and broadened marginally further when the fluence was increased to 1×10^{17} ions/cm^2. However, no obvious broadening of diffraction peak could be observed in A/ANLs 25 [Fig. 1(c)] until the ion fluence was up to 1×10^{17} ions/cm^2 while no such broadening could be observed in A/ANLs 5 [Fig. 1(d)]. Moreover, no crystalline peak could be observed in the patterns of both A/ANLs 25 and A/ANLs 5 after irradiation. This suggested that the A/ANLs exhibited better irradiation resistance than the corresponding single-layered ones, and the more A/A interfaces they contain, the better irradiation resistance they have, as the broadening of diffraction peak indicates the increasing of atomic disorder in materials [27].

Cross-sectional TEM images and the corresponding selected area electron diffraction (SAED) patterns of unirradiated ZrCu, ZrCuNiAlSi, A/ANLs 25 and A/ANLs 5 samples were presented in Fig. 2. In line with the XRD results, the unirradiated ZrCu, ZrCuNiAlSi and their A/ANLs samples exhibited pure amorphous nature, as only one diffuse halo without any crystalline spot could be observed in each inserted SAED pattern in Fig. 2(a)–(d). The corresponding HRTEM images of Fig. 2(e)–(h) further confirmed the amorphous nature of these unirradiated samples. Meanwhile, the A/ANLs exhibited obvious alternating layers with clear A/A interfaces, as shown in Fig. 2(c) and (d). As further revealed by the corresponding HRTEM images, A/A interfaces were straight and smooth in A/ANLs 25 [Fig. 2(g)] but relatively vague and intermixed in A/ANLs 5 [Fig. 2(h)]. Note that, according to the EDS analysis (not shown here for brevity), the dark and bright layers were referred to ZrCu and ZrCuNiAlSi, respectively.

Fig. 3(a) showed the dark field cross-sectional TEM images of the irradiated ZrCu sample at the ion fluence of 1×10^{17} ions/cm^2. Obvious crystalline grains of ~ dozens of nanometer in size were formed in the peak irradiated region (indicated by circle) and sporadic smaller crystalline grains of ~ several nanometers in size were also formed in other regions (indicated by red and white arrows, respectively). The corresponding HRTEM image and SAED pattern of the peak irradiated region shown in Fig. 3(b) further confirmed the formation of crystalline phase referred to here as $Cu_{10}Zr_7$ and $CuZr_2$. This was consistent with previous studies that the stable $Cu_{10}Zr_7$ and $CuZr_2$ phases were more likely to form in Zr-based amorphous alloys after irradiation, due to the enhanced atomic mobility as a result of increased free volume [17,34,36]. Actually, tiny nanocrystallites with grain size of 1–2 nm had already formed in the peak irradiated region of the irradiated ZrCu sample at lower ion fluence, as indicated by yellow arrows in the HRTEM image of Fig. 3(c). This was also reflected by the tiny crystalline spots in the inserted SAED pattern. These results were consistent with the XRD patterns [Fig. 1(a)], as tiny nanocrystallites in the irradiated ZrCu sample at lower ion fluence might be beyond the detecting range of XRD analysis.

Fig. 4 presented representative cross-sectional TEM and HRTEM images of ZrCuNiAlSi amorphous thin film after irradiation with different ion fluencies. In sharp contrast to the ZrCu sample, no crystalline phase was formed in ZrCuNiAlSi after irradiation, since no lattice fringe (or crystalline spot) could be observed in the HRTEM images (or the corresponding SAED patterns) of Fig. 4(b) and (c). This was also in line with the XRD results and further confirmed the better irradiation resistance of ZrCuNiAlSi relative to ZrCu, which should be attributed to the higher glass-forming ability and better thermal stability of the former [33].

Similar to the ZrCuNiAlSi amorphous thin film, both A/ANLs 25 and A/ANLs 5, though containing ZrCu amorphous layers, displayed no crystalline phase after irradiation, as no lattice fringe (or crystalline spot) could be observed in the TEM images (or the corresponding SAED patterns) shown in Figs. 5 and 6. There were nonetheless subtle discrepancies of microstructural evolution upon ion irradiation between

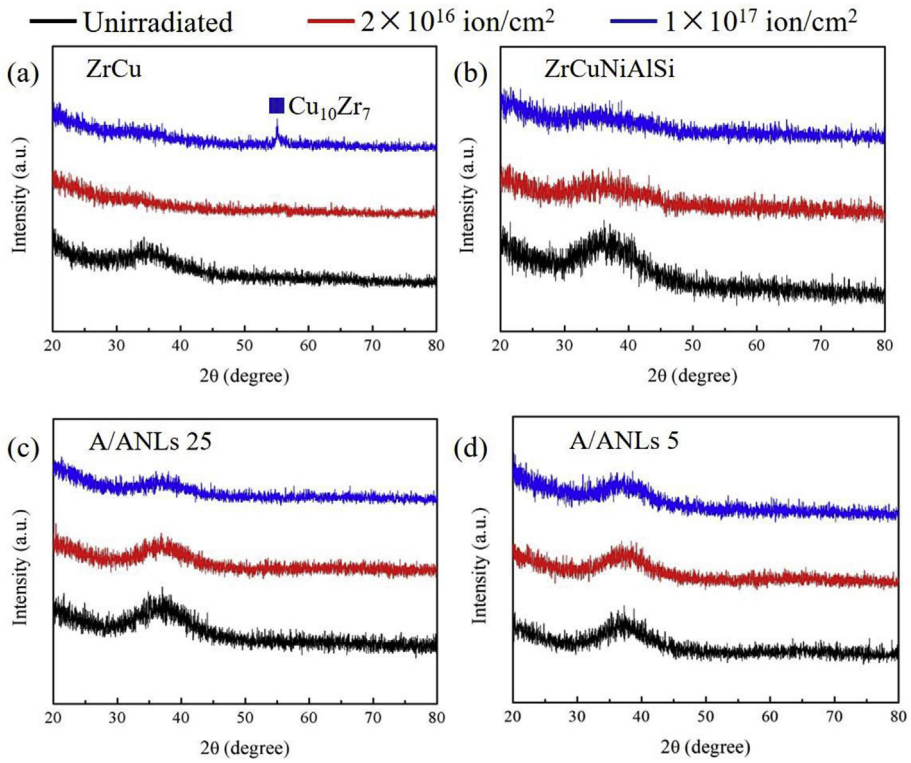

Fig. 1. XRD patterns of (a) ZrCu, (b) ZrCuNiAlSi, (c) A/ANLs 25 and (d) A/ANLs 5 samples before and after He ions irradiation under different ion fluences.

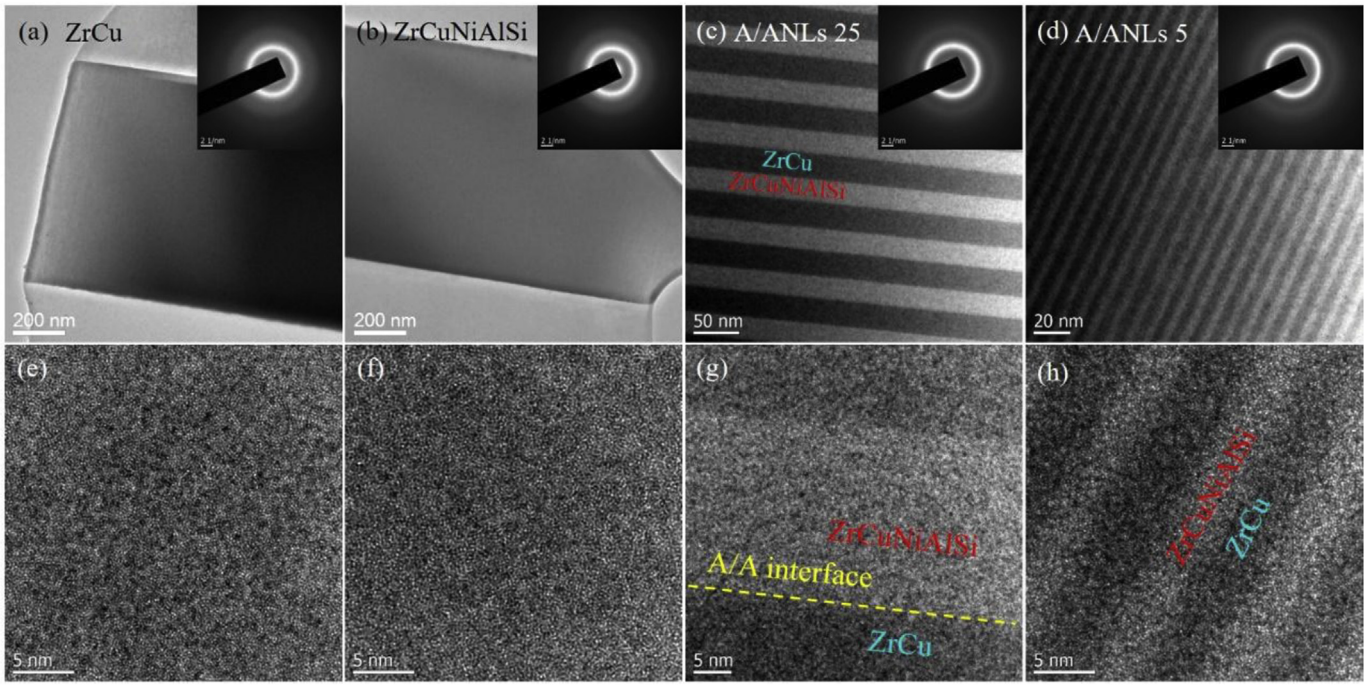

Fig. 2. Bright field cross-sectional TEM images of unirradiated (a) ZrCu, (b) ZrCuNiAlSi, (c) A/ANLs 25 and (d) A/ANLs 5 samples, and their corresponding HRTEM images in (e), (f), (g) and (h). Inserts in (a), (b), (c) and (d) showed the corresponding SAED patterns.

A/ANLs 25 and A/ANLs 5. Particularly, compared with the clear and straight A/A interfaces in the original A/ANLs 25 shown in Fig. 2(g), the A/A interfaces were apparently more vague and intermixed after irradiation as shown in Fig. 5(b) and (c). Moreover, the vagueness and intermixing of A/A interfaces in A/ANLs 25 seemed to increase with increasing irradiation ion fluence, as the contrast between ZrCu and ZrCuNiAlSi layers decreased with increasing ion fluence, indicating radiation-induced atomic mixture occurred. It echoed the XRD results shown in Fig. 1 that radiation-induced atomic mixture should be responsible for the broadening of diffraction peak, though such atomic mixture could be hardly detected in the TEM images of single-layered ZrCu and ZrCuNiAlSi shown in Figs. 3 and 4. In contrast, ion irradiation seemed to have much less impact on the vagueness and intermixing of A/A interfaces in A/ANLs 5, as the features of A/A interfaces in A/ANLs

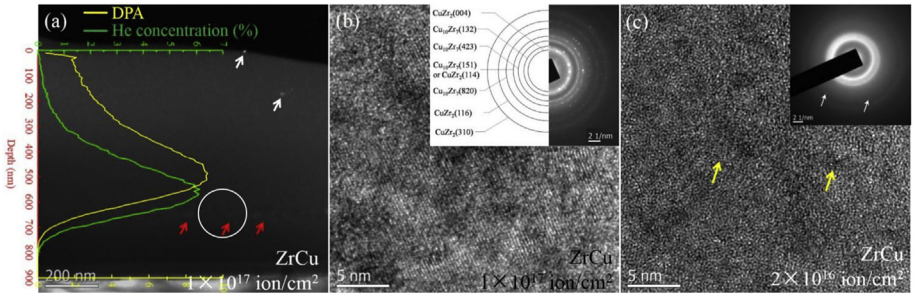

Fig. 3. Representative cross-sectional TEM and HRTEM images of ZrCu amorphous thin films after irradiation with different ion fluences. (a) Dark field cross-sectional TEM images of ZrCu sample after irradiation with an ion fluence of 1×10^{17} ions/cm^2. (b) HRTEM image of the peak irradiated region (indicated by circle) in (a). (c) HRTEM image of the peak irradiated region after irradiation with an ion fluence of 2×10^{16} ions/cm^2. Inserts in (b) and (c) showed the corresponding SAED patterns.

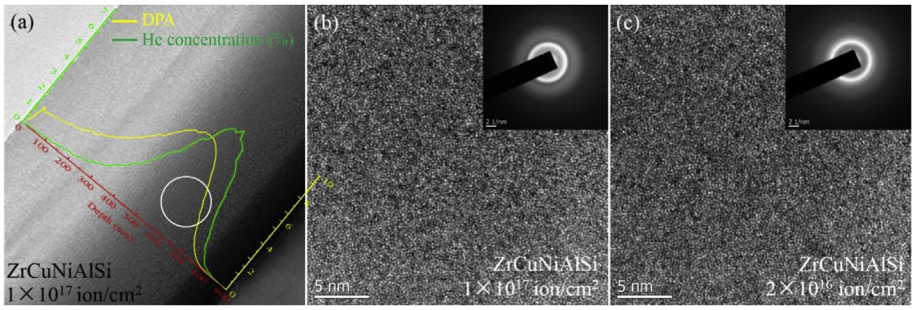

Fig. 4. Representative cross-sectional TEM and HRTEM images of ZrCuNiAlSi amorphous thin films after irradiation with different ion fluences. (a) Bright field cross-sectional TEM images of ZrCuNiAlSi after irradiation with an ion fluence of 1×10^{17} ions/cm^2. (b) HRTEM image of the peak irradiated region (indicated by circle) in (a). (c) HRTEM image of the peak irradiated region after irradiation with an ion fluence of 2×10^{16} ions/cm^2. Inserts in (b) and (c) showed the corresponding SAED patterns.

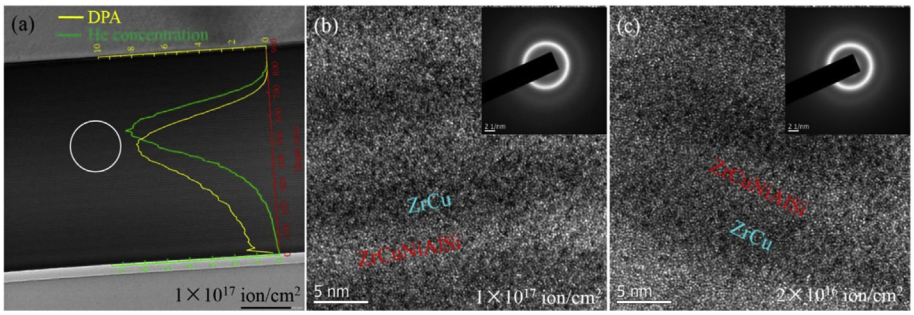

Fig. 5. Representative cross-sectional TEM and HRTEM images of A/ANLs 25 after irradiation with different ion fluences. (a) Bright field cross-sectional TEM images of A/ANLs 25 after irradiation with an ion fluence of 1×10^{17} ions/cm^2. (b) HRTEM image of the peak irradiated region (indicated by circle) in (a). (c) HRTEM image of the peak irradiated region after irradiation with an ion fluence of 2×10^{16} ions/cm^2. Inserts in (b) and (c) showed the corresponding SAED patterns.

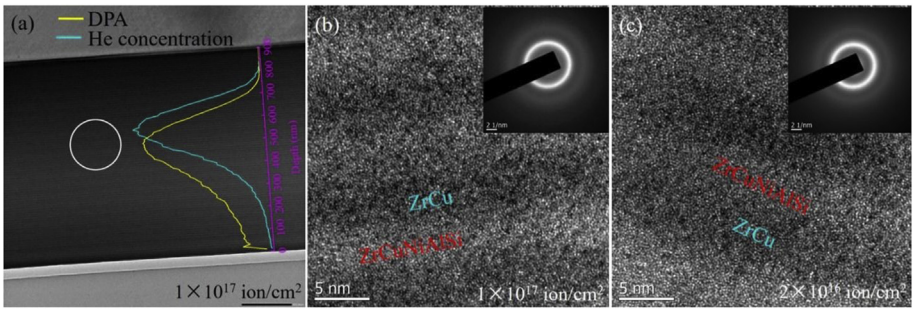

Fig. 6. Representative cross-sectional TEM and HRTEM images of A/ANLs 5 after irradiation with different ion fluences. (a) Bright field cross-sectional TEM images of A/ANLs 5 after irradiation with an ion fluence of 1×10^{17} ions/cm^2. (b) HRTEM image of the peak irradiated region (indicated by circle) in (a). (c) HRTEM image of the peak irradiated region after irradiation with an ion fluence of 2×10^{16} ions/cm^2. Inserts in (b) and (c) showed the corresponding SAED patterns.

5 were quite similar before [Fig. 2(h)] and after ion irradiation [Fig. 6(b) and (c)]. This was also well consistent with the XRD results that A/ANLs 5 possessed better irradiation resistance than A/ANLs 25.

To further characterize the microstructural evolution of ZrCu, ZrCuNiAlSi and their A/ANLs upon He ion irradiation, the radius of the inner diffraction halo in the SAED patterns (R_i), which is inversely related to the inter-atomic distance of materials [27], was determined using the Gatan Digital Micrographs software for the four samples before and after irradiation. The representative method for measuring R_i was shown in Fig. 7(a) and the measured R_i values of both unirradiated and irradiated samples were summarized in Fig. 7(b) (Note that the R_i value was the average value of three SAED patterns of the peak irradiated regions). More detailed information regarding the determination of R_i for each sample was provided in the Supplementary Materials. It could be seen that the R_i of ZrCu increased firstly upon irradiation at a fluence of 2×10^{16} ions/cm^2 and then decreased as the fluence was increased to 1×10^{17} ions/cm^2. This suggested that the ZrCu shrinked firstly and then expanded as the fluence was increased. In comparison, the R_i of ZrCuNiAlSi decreased sharply when irradiated with a lower fluence and then decreased steadily when the fluence was increased to a higher level. This implied a sharp expansion of the ZrCuNiAlSi upon irradiation, and the expansion continued with increasing fluence. In contrast, for both the A/ANLs, the R_i gradually decreased (with a much minor level) as fluence was increased, further indicating the better irradiation resistance of the A/ANLs. Meanwhile, the R_i of A/ANLs 5 was even more stable than A/ANLs 25 upon irradiation, reconfirming that the A/ANLs 5 possessed better irradiation resistance than the A/ANLs 25.

The He bubble morphologies of ZrCu, ZrCuNiAlSi, A/ANLs 25 and A/ANLs 5 samples after irradiation were displayed in Fig. 8. In

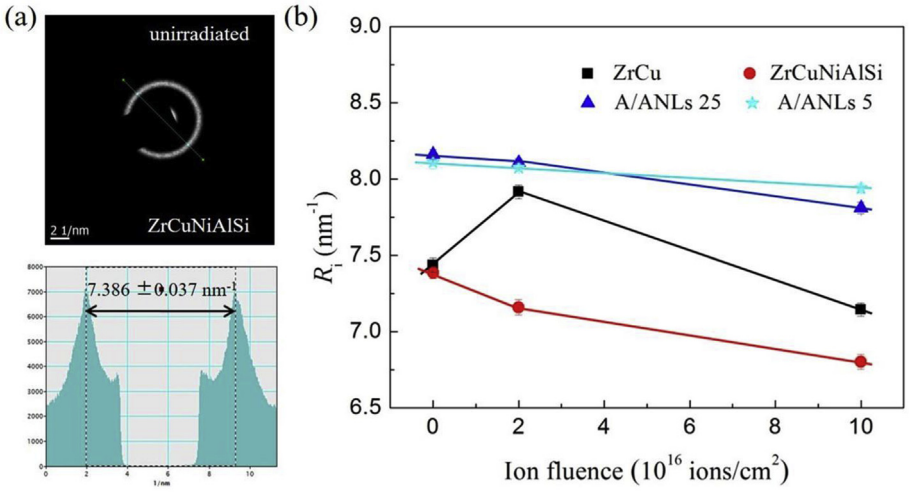

Fig. 7. (a) Representative method for measuring R_i in unirradiated ZrCuNiAlSi and (b) the R_i values of ZrCu, ZrCuNiAlSi, A/ANLs 25 and A/ANLs 5 plotted as functions of ion fluence.

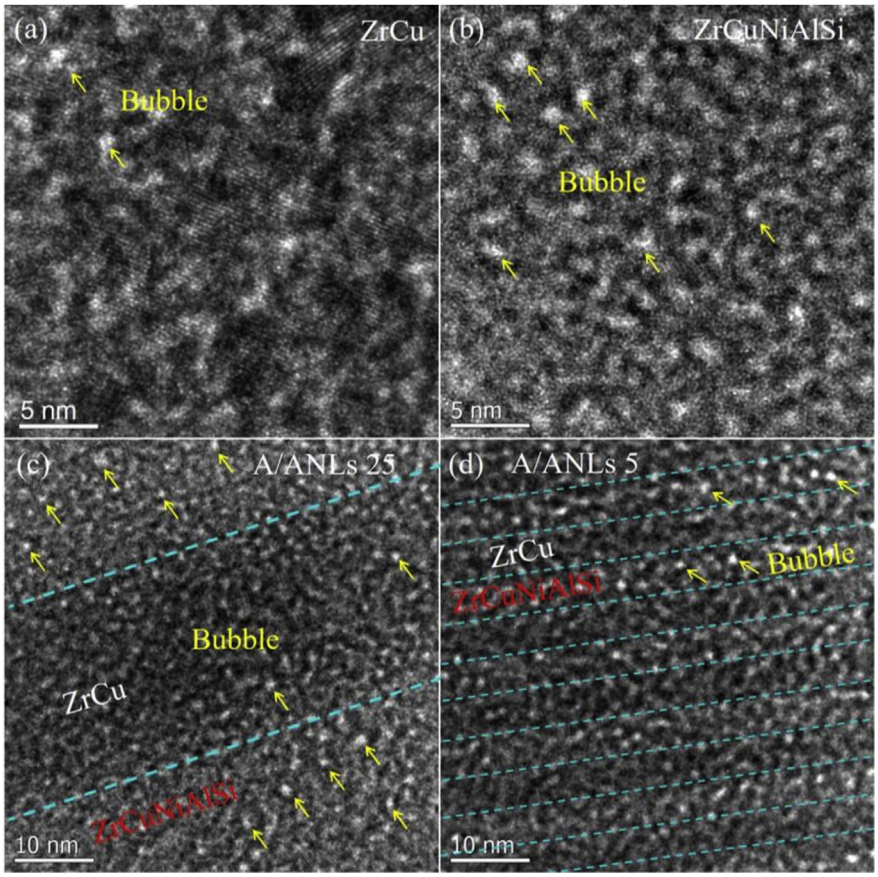

Fig. 8. HRTEM images of the peak irradiated region in (a) ZrCu, (b) ZrCuNiAlSi, (c) A/ANLs 25 and (d) A/ANLs 5with an ion fluence of 1×10^{17} ions/cm^2 under-focus of 500 nm.

agreement with existing studies [17,24,37], the He bubbles were shown as white dots indicated by arrows in the HRTEM images of under-focus. Upon irradiation, less He bubbles formed in ZrCu [Fig. 8(a)] than in ZrCuNiAlSi [Fig. 8(b)] and He bubbles were sporadically distributed in or beside the crystalline lattice in ZrCu. Accordingly, for both A/ANLs 25 and A/ANLs 5, less and smaller He bubbles formed in ZrCu than in ZrCuNiAlSi, as shown in Fig. 8(c) and (d). Meanwhile, the A/ANLs 5 [Fig. 8(d)] had fewer He bubbles compared with the A/ANLs 25 [Fig. 8(c)] and such contrast was especially strong in their ZrCu layers, thus revealing the sink effect of A/A interfaces for He bubbles. Moreover, the remaining He bubbles in both A/ANLs were mostly located at the central part of each layer, indicating that the interface-affected zones might exist.

Upon irradiation, whether an amorphous alloy would undergo crystallization is dependent of its intrinsic properties (such as glass-forming ability and thermal stability) and extrinsic irradiation conditions (such as irradiation energy, dose, temperature and pressure) [25]. Under identical irradiation conditions, amorphous alloys with higher

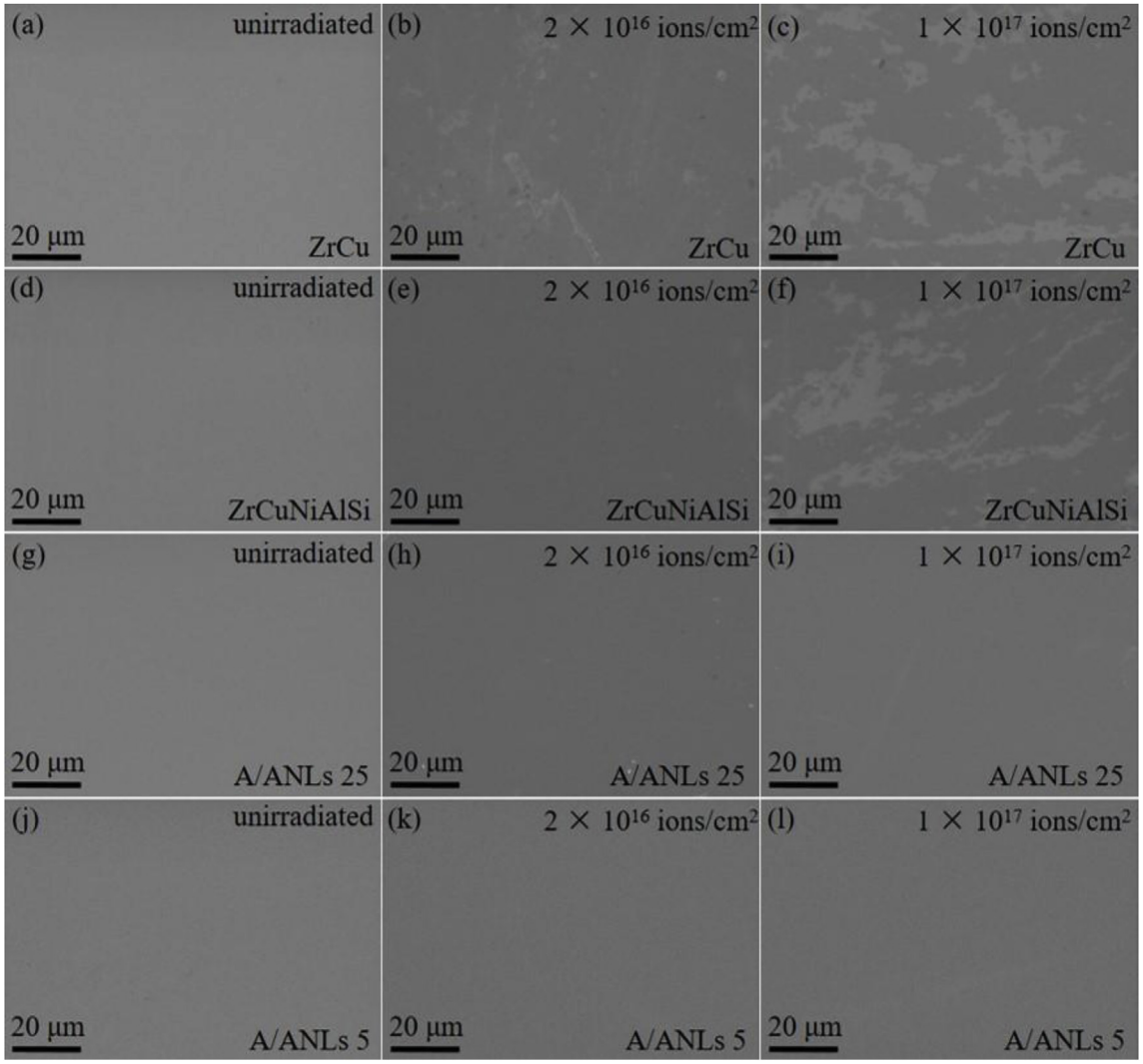

Fig. 9. Surface morphologies of (a)–(c) ZrCu, (d)–(f) ZrCuNiAlSi, (g)–(i) A/ANLs 25, and (j)–(l) A/ANLs 5 before and after He ions irradiation with different ion fluencies.

glass-forming ability and better thermal stability always exhibit better resistance to crystallization [24,34]. That is why crystallization happened in ZrCu rather than ZrCuNiAlSi, as the quinary ZrCuNiAlSi possesses higher glass-forming ability and better thermal stability than the binary ZrCu [33]. However, the present A/ANLs samples with plenty of ZrCu layers both displayed no crystallization after irradiation (Figs. 5 and 6). Consequently, in these A/ANLs, A/A interfaces may play a crucial role in suppressing crystallization in ZrCu layers.

Crystallization is a thermal activation process and hence may happen only when the activation energy barrier is overcome [38]. It was demonstrated that ion irradiation can induce "defects" (termed as the free volume [27] or the liquid-like zone [39]) in amorphous alloys, which was also verified by the radiation-induced expansion (*i.e.*, reduction of R_i) of the present samples in Fig. 7. Note that the shrink in ZrCu irradiated at an ion fluence of 2×10^{16} ions/cm^2 should be ascribed to crystallization, while radiation-induced expansion surpassed shrink due to crystallization at the ion fluence of 1×10^{17} ions/cm^2. The radiation-induced "defects" may increase the Gibbs free energy (correspondingly, reduce the activation energy barrier for crystallization) and also provide numerous nucleation sites for crystallization [24], thus facilitating the occurrence of crystallization [20]. In the present A/ANLs, similar to C/C and A/C interfaces, the A/A interfaces may serve as "defect" sinks, as their sink effect for He bubbles was confirmed by the He bubbles morphology of Fig. 8 and, to certain extent, the He bubbles may indicate free volume regions [24]. Therefore, the presence of abundant A/A interfaces may greatly reduce the amount of "defects" in both ZrCu and ZrCuNiAlSi layers, which in turn alleviates radiation-induced crystallization in ZrCu layers.

Interfacial stresses may also affect crystallization in A/ANLs. As crystallization of an amorphous alloy will lead to shrinking of its volume or dimension, crystallization should be promoted under compressive stressing and suppressed under tensile stressing [20]. As shown in Fig. 8, more He bubbles formed in ZrCuNiAlSi layers than in CuZr, which may bring larger expansion in the former than the latter, hence resulting in tensile stressing in CuZr and compressive stressing in ZrCuNiAlSi.

Therefore, the A/A interfaces in A/ANLs were responsible for the suppression of crystallization in ZrCu via absorption of radiation-induced "defects" and interface stresses. Meanwhile, by assimilating radiation-induced "defects", the A/A interfaces also contributed to stabilize the microstructure of amorphous alloys, resulting in the better irradiation resistance of A/ANLs than ZrCu and ZrCuNiAlSi. Accordingly, A/ANLs 5 with more A/A interfaces possessed better irradiation resistance than A/ANLs 25. It should be noticed that, similar to the situation in C/C interfaces that the incoherent ones have higher sink strength than the coherent ones due to their higher content of free volume [14–16], the more intermixed interfaces in A/ANLs 5 may have higher sink strength than the smooth ones in A/ANLs 25, which might

also contribute to the better irradiation resistance of A/ANLs 5 relative to A/ANLs 25.

3.2. Surface morphology evolution of ZrCu, ZrCuNiAlSi and their A/ANLs under He irradiation

Fig. 9 presented the surface morphologies (examined by SEM observation) of ZrCu, ZrCuNiAlSi and their A/ANLs before and after He ions irradiation with different ion fluencies. The surfaces of the four samples were essentially featureless in the original state as shown in Fig. 9(a), (d), (g), and (j), but their responses to irradiation were quite different. Particularly, cracking and spalling could be observed on the surface of ZrCu at the ion fluence of 2×10^{16} ions/cm^2 [Fig. 9(b)], which became more severe when the fluence was increased to 1×10^{17} ions/cm^2 [Fig. 9(c)]. Obvious surface damage could only be observed after high dose irradiation for ZrCuNiAlSi [Fig. 9(f)], as its surface remained smooth at low dose [Fig. 9(e)]. In contrast, no apparent radiation-induced damage could be observed on the surfaces of both A/ANLs 25 [Fig. 9(h) and (i)] and A/ANLs 5 [Fig. 9(k) and (l)]. This further confirmed that A/ANLs possessed better irradiation resistance than ZrCu and ZrCuNiAlSi.

As we all know that the formation of He bubbles will generate extrusion and stress among the atoms in amorphous alloys. When the concentration of He atoms exceeds the threshold for amorphous alloys to dissolve, surface damage such as cracking and spalling would occur. The He atoms solubility of an amorphous alloy may be represented by the magnitude of ion fluence needed to induce surface damage during irradiation [24]. Therefore, ZrCu has lower He atoms solubility than ZrCuNiAlSi, since its surface started to crack at lower ion fluence. For the ZrCu/ZrCuNiAlSi A/ANLs, with the help of A/A interfaces that effectively absorbed the He bubbles, their He atoms solubility was greatly enhanced such that no surface damage happened even at relatively high ion fluence.

4. Conclusion

It was experimentally demonstrated that ZrCu/ZrCuNiAlSi A/ANLs had preferable irradiation resistance relative to ZrCu and ZrCuNiAlSi single-layered amorphous thin films, as the former exhibited better microstructure stability and higher He ion solubility than the latter during He ion irradiation. Particularly, radiation-induced crystallization and obvious expansion happened in ZrCu and ZrCuNiAlSi, respecitively, but not in A/ANLs; surface damages like cracking and spalling were observed in ZrCu and ZrCuNiAlSi rather than in A/ANLs after irradiation. Besides, A/ANLs 5 exhibited even better microstructure stability than A/ANLs 25 after irradiation. These results were attributed to the significant influence of A/A interfaces, which served as sinks to assimilate radiation-induced “defects” and He bubbles during irradiation, suppressing therefore the crystallization, stabilizing the microstructure and preventing the occurrence of surface damages in A/ANLs. This study provides new insights into the design and development of irradiation resistance materials.

Acknowledgements

P. Huang acknowledges financial support from the National Natural Science Foundation of China (No.51471131), Z. Q. Chen acknowledges financial support from Fundamental Research Funds for the Central Universities (No. 021314380118) and F. Wang acknowledges financial support from Fundamental Research Funds for the Central Universities.

Appendix A. Supplementary data

Supplementary data to this article can be found online at https://doi.org/10.1016/j.intermet.2019.01.007.

References

[1] S.J. Zinkle, G.S. Was, Materials challenges in nuclear energy, Acta Mater. 61 (2013) 735–758.
[2] S.J. Zinkle, J.T. Busby, Structural materials for fission & fusion energy, Mater. Today 12 (2009) 12–19.
[3] P. Hosemann, D. Frazer, M. Fratoni, A. Bolind, M.F. Ashby, Materials selection for nuclear applications: challenges and opportunities, Scripta Mater. 143 (2018) 181–187.
[4] S. Mao, S. Shu, J. Zhou, R.S. Averback, S.J. Dillon, Quantitative comparison of sink efficiency of Cu–Nb, Cu–V and Cu–Ni interfaces for point defects, Acta Mater. 82 (2015) 328–335.
[5] E.G. Fu, A. Misra, H. Wang, L. Shao, X. Zhang, Interface enabled defects reduction in helium ion irradiated Cu/V nanolayers, J. Nucl. Mater. 407 (2010) 178–188.
[6] N. Li, J.J. Carter, A. Misra, L. Shao, H. Wang, X. Zhang, The influence of interfaces on the formation of bubbles in He-ion-irradiated Cu/Mo nanolayers, Phil. Mag. Lett. 91 (2011) 18–28.
[7] Y. Gao, T. Yang, J. Xue, S. Yan, S. Zhou, Y. Wang, D.T.K. Kwok, P.K. Chu, Y. Zhang, Radiation tolerance of Cu/W multilayered nanocomposites, J. Nucl. Mater. 413 (2011) 11–15.
[8] N. Li, M.S. Martin, O. Anderoglu, A. Misra, L. Shao, H. Wang, X. Zhang, He ion irradiation damage in Al/Nb multilayers, J. Appl. Phys. 105 (2009) 123522.
[9] Q.M. Wei, N. Li, N. Mara, M. Nastasi, A. Misra, Suppression of irradiation hardening in nanoscale V/Ag multilayers, Acta Mater. 59 (2011) 6331–6340.
[10] H.L. Heinisch, F. Gao, R.J. Kurtz, The effects of interfaces on radiation damage production in layered metal composites, J. Nucl. Mater. 329–333 (2004) 924–928.
[11] Y. Chen, Y. Liu, E.G. Fu, C. Sun, K.Y. Yu, M. Song, J. Li, Y.Q. Wang, H. Wang, X. Zhang, Unusual size-dependent strengthening mechanisms in helium ion-irradiated immiscible coherent Cu/Co nanolayers, Acta Mater. 84 (2015) 393–404.
[12] K.Y. Yu, Y. Liu, E.G. Fu, Y.Q. Wang, M.T. Myers, H. Wang, L. Shao, X. Zhang, Comparisons of radiation damage in He ion and proton irradiated immiscible Ag/Ni nanolayers, J. Nucl. Mater. 440 (2013) 310–318.
[13] N. Li, E.G. Fu, H. Wang, J.J. Carter, L. Shao, S.A. Maloy, A. Misra, X. Zhang, He ion irradiation damage in Fe/W nanolayer films, J. Nucl. Mater. 389 (2009) 233–238.
[14] X. Zhang, E.G. Fu, A. Misra, M.J. Demkowicz, Interface-enabled defect reduction in He ion irradiated metallic multilayers, JOM 62 (2010) 75–78.
[15] X. Zhang, E.G. Fu, N. Li, A. Misra, Y.Q. Wang, L. Shao, H. Wang, Design of radiation tolerant nanostructured metallic multilayers, J. Eng. Mater. Technol. 134 (2012) 041010-1-041010-9.
[16] M.J. Demkowicz, R.G. Hoagland, J.P. Hirth, Interface structure and radiation damage resistance in Cu-Nb multilayer nanocomposites, Phys. Rev. Lett. 100 (2008) 136102.
[17] J.Y. Zhang, Y.Q. Wang, X.Q. Liang, F.L. Zeng, G. Liu, J. Sun, Size-dependent He-irradiated tolerance and plastic deformation of crystalline/amorphous Cu/Cu–Zr nanolaminates, Acta Mater. 92 (2015) 140–151.
[18] Q. Su, L. Price, J.A. Colon Santana, L. Shao, M. Nastasi, Irradiation tolerance of amorphous SiOC/crystalline Fe composite, Mater. Lett. 155 (2015) 138–141.
[19] K.Y. Yu, Z. Fan, Y. Chen, M. Song, Y. Liu, H. Wang, M.A. Kirk, M. Li, X. Zhang, In situ observation of defect annihilation in Kr ion-irradiated bulk Fe/amorphous-Fe_2Zr nanocomposite alloy, Mater. Res. Lett. 3 (2014) 35–42.
[20] Y. Chen, L. Jiao, C. Sun, M. Song, K.Y. Yu, Y. Liu, M. Kirk, M. Li, H. Wang, X. Zhang, In situ studies of radiation induced crystallization in Fe/a-Y_2O_3 nanolayers, J. Nucl. Mater. 452 (2014) 321–327.
[21] O. Anderoglu, M.J. Zhou, J. Zhang, Y.Q. Wang, S.A. Maloy, J.K. Baldwin, A. Misra, He^+ ion irradiation response of Fe–TiO_2 multilayers, J. Nucl. Mater. 435 (2013) 96–101.
[22] C. Schuh, T. Hufnagel, U. Ramamurty, Mechanical behavior of amorphous alloys, Acta Mater. 55 (2007) 4067–4109.
[23] T.C. Hufnagel, C.A. Schuh, M.L. Falk, Deformation of metallic glasses: recent developments in theory, simulations, and experiments, Acta Mater. 109 (2016) 375–393.
[24] X.N. Zhang, X.X. Mei, Q. Zhang, X.N. Li, J.B. Qiang, Y.N. Wang, Damage induced by helium ion irradiation in Fe-based metallic glass, J. Nucl. Mater. 490 (2017) 216–225.
[25] A.G. Perez-Bergquist, H. Bei, K.J. Leonard, Y. Zhang, S.J. Zinkle, Effects of ion irradiation on Zr52.5Cu17.9Ni14.6Al10Ti5 (BAM-11) bulk metallic glass, Intermetallics 53 (2014) 62–66.
[26] Y. Huang, H. Fan, X. Zhou, P. Xue, Z. Ning, D. Daisenberger, J. Sun, J. Shen, Structure and mechanical property modification of a Ti-based metallic glass by ion irradiation, Scripta Mater. 103 (2015) 41–44.
[27] X.L. Bian, G. Wang, H.C. Chen, L. Yan, J.G. Wang, Q. Wang, P.F. Hu, J.L. Ren, K.C. Chan, N. Zheng, A. Teresiak, Y.L. Gao, Q.J. Zhai, J. Eckert, J. Beadsworth, K.A. Dahmen, P.K. Liaw, Manipulation of free volumes in a metallic glass through Xe-ion irradiation, Acta Mater. 106 (2016) 66–77.
[28] R.L. Thompson, Y. Wang, J.R. Greer, Irradiation enhances strength and deformability of nano-architected metallic glass, Adv. Eng. Mater. 20 (2018) 1701055.
[29] X. Zhou, C. Chen, Strengthening and toughening mechanisms of amorphous/amorphous nanolaminates, Int. J. Plast. 80 (2016) 75–85.
[30] C. Zhong, H. Zhang, Q.P. Cao, X.D. Wang, D.X. Zhang, J.W. Hu, P.K. Liaw, J.Z. Jiang, Non-localized deformation in Cu-Zr multi-layer amorphous films under tension, J. Alloy. Comp. 678 (2016) 410–420.
[31] P. Sharma, K. Yubuta, H. Kimura, A. Inoue, Brittle metallic glass deforms plastically at room temperature in glassy multilayers, Phys. Rev. B 80 (2009) 024106.
[32] A. Inoue, A. Takeuchi, Recent development and application products of bulk glassy alloys, Acta Mater. 59 (2011) 2243–2267.

[33] W.H. Wang, C. Dong, C.H. Shek, Bulk metallic glasses, Mater. Sci. Eng. R. 44 (2004) 45–89.
[34] E.G. Fu, J. Carter, M. Martin, G. Xie, X. Zhang, Y.Q. Wang, R. Littleton, L. Shao, Electron irradiation-induced structural transformation in metallic glasses, Scripta Mater. 61 (2009) 40–43.
[35] J.P. Biersack, J.F. Ziegler, The Stopping and Range of Ions in Solids, Pergamon (1985).
[36] J. Carter, M. Martin, G.Q. Xie, X. Zhang, Y.Q. Wang, D. Wijesundera, X.M. Wang, W.K. Chu, L. Shao, Effects of Cu ion irradiation in Cu50Zr45Ti5 metallic glass, Scripta Mater. 61 (2009) 265–268.
[37] R. Liontas, X.W. Gu, E. Fu, Y. Wang, N. Li, N. Mara, J.R. Greer, Effects of helium implantation on the tensile properties and microstructure of Ni73P27Metallic glass nanostructures, Nano Lett. 14 (2014) 5176–5183.
[38] K. Lu, Nanocrystalline metals crystallized from amorphous solids: nanocrystallization, structure, and properties, Mater. Sci. Eng. R. 16 (1996) 161–221.
[39] K. Zhang, Z. Hu, Z. Zhao, B. Wei, Y. Li, Y. Wei, Whiskers growth and self-healing in Ti-based metallic glasses during ion irradiation, Appl. Surf. Sci. 437 (2018) 176–180.